

Experimental tests of the Weinberg–Salam theory

13.1 The search for the gauge bosons

We saw in the preceding chapter that the low energy limit of the electroweak Weinberg–Salam theory reduces to the successful phenomenology of Chapter 9. There is no reason to doubt that the Weinberg–Salam theory describes all low energy β decays, but it also describes very much more. The pathological cross-section of equation (9.14) is modified to

$$\sigma(\nu_\mu e^- \rightarrow \mu^- \nu_e) = \frac{G_F^2}{\pi} \left(\frac{(s - m_\mu^2)^2}{s[1 + (s - m_\mu^2)/M_w^2]} \right). \quad (13.1)$$

At high energies $\gg M_w$, this expression tends to $G_F^2 M_w^2 / \pi = 1.08 \times 10^{-10}$ b. It is a renormalisable theory, so that quantum corrections can be calculated. At high energies these corrections become increasingly important (at the few per cent level).

The clearest test of the theory is the observation of the conjectured gauge bosons, the W^\pm and Z . These were discovered at CERN in 1983, using a specially constructed proton–antiproton collider, with a centre of mass energy of 540 GeV. It was very important for the successful identification of the new particles that their masses and decay characteristics had already been well estimated within the theory. The masses depend on G_F , e and the Weinberg angle θ_w (equations (11.37) and (12.22)). The values of G_F and e were well established, and estimates of θ_w were available from careful observations of neutral current events. We saw in Section 12.3 that the $e\nu_\mu \rightarrow e\nu_\mu$ and $e\bar{\nu}_\mu \rightarrow e\bar{\nu}_\mu$ cross-sections are sensitive to θ_w . Similarly, the cross-sections for ν and $\bar{\nu}$ scattering from nuclei depend on θ_w , as we shall see in more detail in Chapter 14. Since the centre of mass energy available in neutrino–nuclear scattering is much greater than in neutrino–electron scattering (equation (9.13)) and the cross-sections increase with energy, it was the neutral

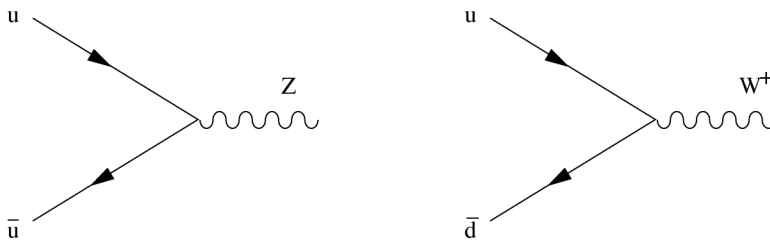


Figure 13.1 Quark–antiquark annihilation is the principal process contributing to W and Z production in proton–antiproton collisions at present day collider energies.

current experiments on nuclei which gave an estimate of θ_w , and this estimate was in fact close to the presently accepted value. The experimental physicists knew what to look for!

The successful identification of the new particles also relied on estimates of the likely production cross-sections of the particles. We have not yet discussed how quarks interact with the W^\pm and Z bosons, but we shall see in Chapter 14 that the interactions are similar to the interactions of leptons with the gauge bosons. Two of the processes that contribute to Z and W^+ production are sketched in Fig. 13.1. The outgoing proton and antiproton remnants materialise as complicated jets of particles moving in directions closely correlated with the original proton and antiproton directions. It is a fortunate circumstance for identification that the decay products of the gauge bosons are frequently well separated from the particles in the remnants (Problem 13.1).

The quark–antiquark pair responsible for gauge boson production carry only a fraction of the original 540 GeV of energy, and the 540 GeV design parameter allowed for this effect. The important analysis of the partition of the energy of a beam particle between its constituents is discussed in Appendix D.

13.2 The W^\pm bosons

The results of these experiments at CERN and subsequent experiments dramatically confirmed the theoretical expectations. The charged W^\pm bosons have a mass

$$M_w = 80.425 \pm 0.038 \text{ GeV},$$

and their decay rates to lepton pairs are measured to be

$$\begin{aligned} \Gamma(W^+ \rightarrow e^+\nu_e) &= 228 \pm 6 \text{ MeV}, \\ \Gamma(W^+ \rightarrow \mu^+\nu_\mu) &= 225 \pm 9 \text{ MeV}, \\ \Gamma(W^+ \rightarrow \tau^+\nu_\tau) &= 228 \pm 11 \text{ MeV}, \end{aligned}$$

and $\Gamma(W^+ \rightarrow e^+\nu_e) = \Gamma(W^- \rightarrow e^-\bar{\nu}_e)$, etc.

To lowest order in perturbation theory, and neglecting terms in $(m_{\text{lepton}}/M_w)^2$, these partial widths are all equal in the Standard Model and

$$\Gamma(W^+ \rightarrow e^+\nu) = \frac{G_F M_W^3}{6\pi\sqrt{2}} = 226 \pm 1 \text{ MeV}, \quad (13.2)$$

(Problem 13.3) in good agreement with the experimental data.

13.3 The Z boson

The experiments that revealed the charged W^\pm bosons also revealed the neutral Z boson, but the mass of the Z boson and its decay rates are now known far more accurately than those of the W^\pm bosons. In 1989, two e^+e^- colliders were opened: LEP at CERN and SLC at Stanford. In these machines, the electrons and positrons have equal energies and opposite momenta, and the centre of mass energy can be tuned to lie at and around the mass of the Z. Typical resonant cross-sections for particle production are shown in Fig. 13.2, and corresponding Feynman diagrams in Fig. 13.3. At the peak energy, Z bosons at rest are copiously produced by e^+e^- annihilation. These very clean events have given precise data on the properties of the Z. The mass of the Z is

$$M_Z = 91.1876 \pm 0.0021 \text{ GeV},$$

and partial decay widths to charged lepton–antilepton pairs are

$$\begin{aligned} \Gamma(Z \rightarrow e^+e^-) &= 83.91 \pm 0.20 \text{ MeV}, \\ \Gamma(Z \rightarrow \mu^+\mu^-) &= 83.99 \pm 0.35 \text{ MeV}, \\ \Gamma(Z \rightarrow \tau^+\tau^-) &= 84.09 \pm 0.40 \text{ MeV}. \end{aligned}$$

The total decay width, which includes decays to hadrons and the $\nu\bar{\nu}$ pairs, is $\Gamma(\text{total}) = 2495 \pm 2 \text{ MeV}$.

The theoretical partial widths for decay to charged lepton pairs depend on the Weinberg angle θ_w . To lowest order and neglecting terms in $(m_{\text{lepton}}/M_z)^2$, the partial widths are all equal and

$$\Gamma(Z \rightarrow e^+e^-) = \frac{G_F M_z^3}{12\sqrt{2}\pi} [(1 - 2\sin^2\theta_w)^2 + 4\sin^4\theta_w]. \quad (13.3)$$

Taking the accepted value of $\sin^2\theta_w = 0.2312$, this gives, to lowest order,

$$\Gamma(Z \rightarrow e^+e^-) = 83.4 \text{ MeV}.$$

Again, there is remarkable agreement between theory and experiment.

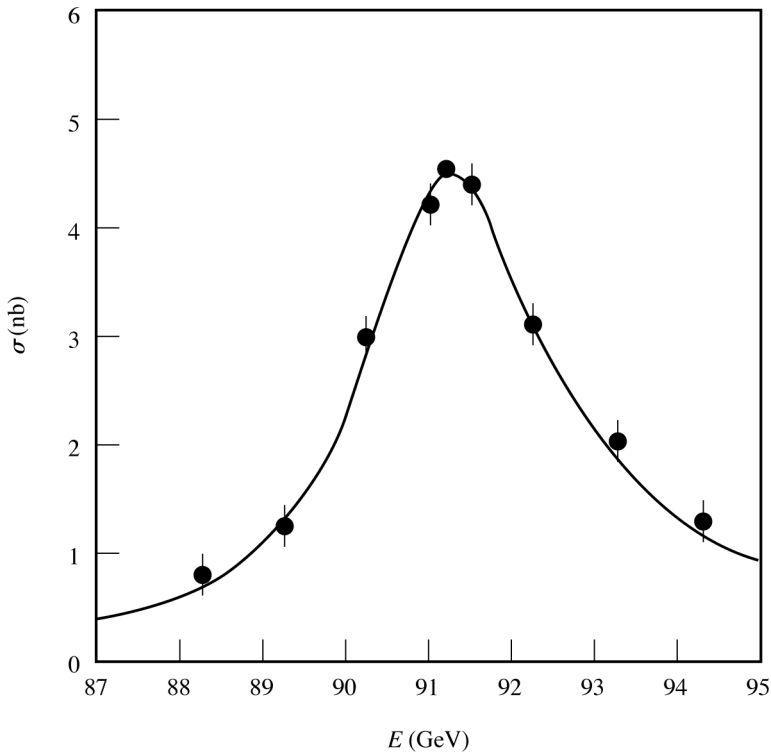


Figure 13.2 The cross-section $\sigma(e^+e^- \rightarrow e^+e^- + \mu^+\mu^- + \tau^+\tau^-)$ as a function of E the initiating e^+e^- centre of mass energy. The experimental data were presented at the 25th International Conference on High Energy Physics in Singapore in 1990 by the ALEPH collaboration of CERN. The curve is the prediction of the Standard Model but with parameters such as the Z mass as variables determined by the data (see Hansen (1991)).

13.4 The number of lepton families

For the decay rates to neutrino–antineutrino pairs, the Standard Model gives

$$\Gamma(Z \rightarrow \nu_e \bar{\nu}_e) = \Gamma(Z \rightarrow \nu_\mu \bar{\nu}_\mu) = \Gamma(Z \rightarrow \nu_\tau \bar{\nu}_\tau) = \frac{G_F M_Z^3}{12\sqrt{2}\pi} = 165.9 \text{ MeV}. \quad (13.4)$$

Hence the partial width for decay to any neutrino–antineutrino pair is

$$3\Gamma(Z \rightarrow \nu_e \bar{\nu}_e) = 497.6 \text{ MeV}.$$

This can be compared with the partial width $\Gamma(\text{invisible})$ associated with e^+e^- pairs annihilating without trace, since neutrinos and antineutrinos are the only particles that will escape unseen by the particle detectors.

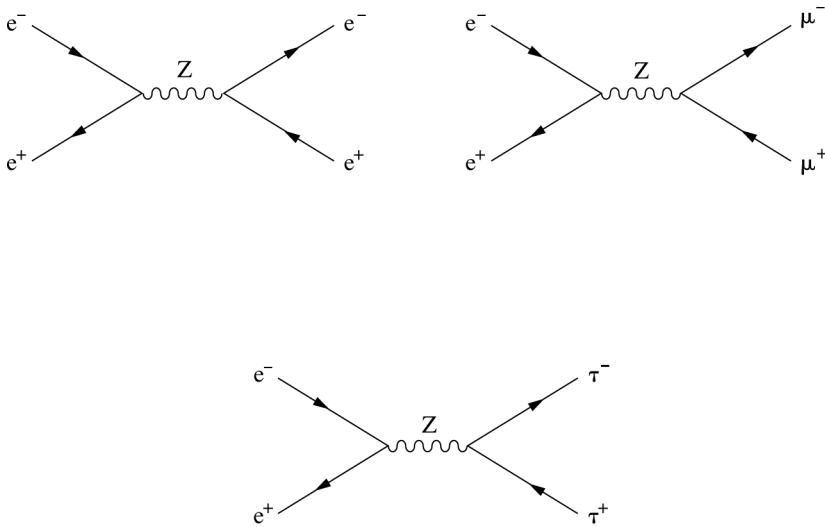


Figure 13.3 The basic Feynman graphs that describe the processes of Fig. 13.2. The fitting curve includes additional graphs that give the Z resonance its width and graphs that describe accompanying electromagnetic processes.

Experimentally, it is found that

$$\Gamma(\text{invisible}) = 498.3 \pm 4.2 \text{ MeV}.$$

The agreement with the Standard Model value is a striking confirmation of the theory. It implies that there are no more light neutrino types and rules out there being any more ‘standard’ lepton doublets in Nature than the three already known. This is a result of fundamental significance.

13.5 The measurement of partial widths

In view of the importance of the partial widths for Z decay, we shall sketch how they are obtained from the experimental results. The cross-section for e^+e^- elastic scattering at small angles is dominated by photon exchange, even around the Z resonance, and is well known from QED. This small angle elastic scattering of the beam particles is constantly monitored during data taking, and the cross-section for any other process, for example $e^+e^- \rightarrow \mu^+\mu^-$, is then obtained from the measured rate of $\mu^+\mu^-$ production relative to the rate of e^+e^- small angle scattering. This, essentially, is how the graphs of Fig. 13.2 are arrived at. We give now a much simplified analysis that indicates how the partial widths are extracted.

Assume that the cross-sections are described by a simple Breit–Wigner formula. For example,

$$\sigma(e^+e^- \rightarrow \mu^+\mu^-) = \frac{3\pi}{M_z^2} \frac{\Gamma_{ee}\Gamma_{\mu\mu}}{(E - M_z)^2 + \Gamma^2/4}, \quad (13.5)$$

$$\sigma(e^+e^- \rightarrow \text{hadrons}) = \frac{3\pi}{M_z^2} \frac{\Gamma_{ee}\Gamma_{\text{had}}}{(E - M_z)^2 + \Gamma^2/4}. \quad (13.6)$$

(The factor 3 is a spin factor.)

M_z and the total decay width Γ can be found from the position and width of the experimental peak. Then, taking $\Gamma_{ee} = \Gamma_{\mu\mu}$, the ratio Γ_{ee}/Γ can be found from the peak of the cross-section $\sigma(e^+e^- \rightarrow \mu^+\mu^-)$ at $E = M_z$, using (13.5):

$$\frac{\Gamma_{ee}}{\Gamma} = \left(\frac{M_z^2 \sigma(e^+e^- \rightarrow \mu^+\mu^- \text{ at } E = M_z)}{12\pi} \right)^{1/2}.$$

Using this result, the ratio $\Gamma_{\text{had}}/\Gamma$ follows from the peak of the cross-section $\sigma(e^+e^- \rightarrow \text{hadrons})$. From (13.6),

$$\frac{\Gamma_{\text{had}}}{\Gamma} = \frac{M_z^2}{12\pi} \frac{\Gamma}{\Gamma_{ee}} \sigma(e^+e^- \rightarrow \text{hadrons at } E = M_z).$$

To obtain $\Gamma(\text{invisible})$, we take

$$\Gamma(\text{invisible}) = \Gamma - 3\Gamma_{ee} - \Gamma_{\text{had}}.$$

In reality the data have to be treated very much more carefully than is implied above. In particular electromagnetic effects during the collision process distort the simple Breit–Wigner shape, and appropriate corrections are applied in the actual analysis.

Figure 13.4 shows the result of such a more sophisticated fit, compared with Standard Model predictions assuming two, three and four types of massless neutrinos. The data unequivocally require three.

13.6 Left–right production cross-section asymmetry and lepton decay asymmetry of the Z boson

Other details of the Weinberg–Salam theory can be tested with e^+e^- colliders. Much work has been done at Stanford with the SLC beam energies tuned to the Z boson mass. The beam intensities at SLC were lower than those at the CERN collider, but the SLC had an advantage in that the electron beam can be polarised along the beam direction so that the relative proportions of positive and negative helicity electrons can be changed. We have seen in Chapter 7 that, at high energies, negative

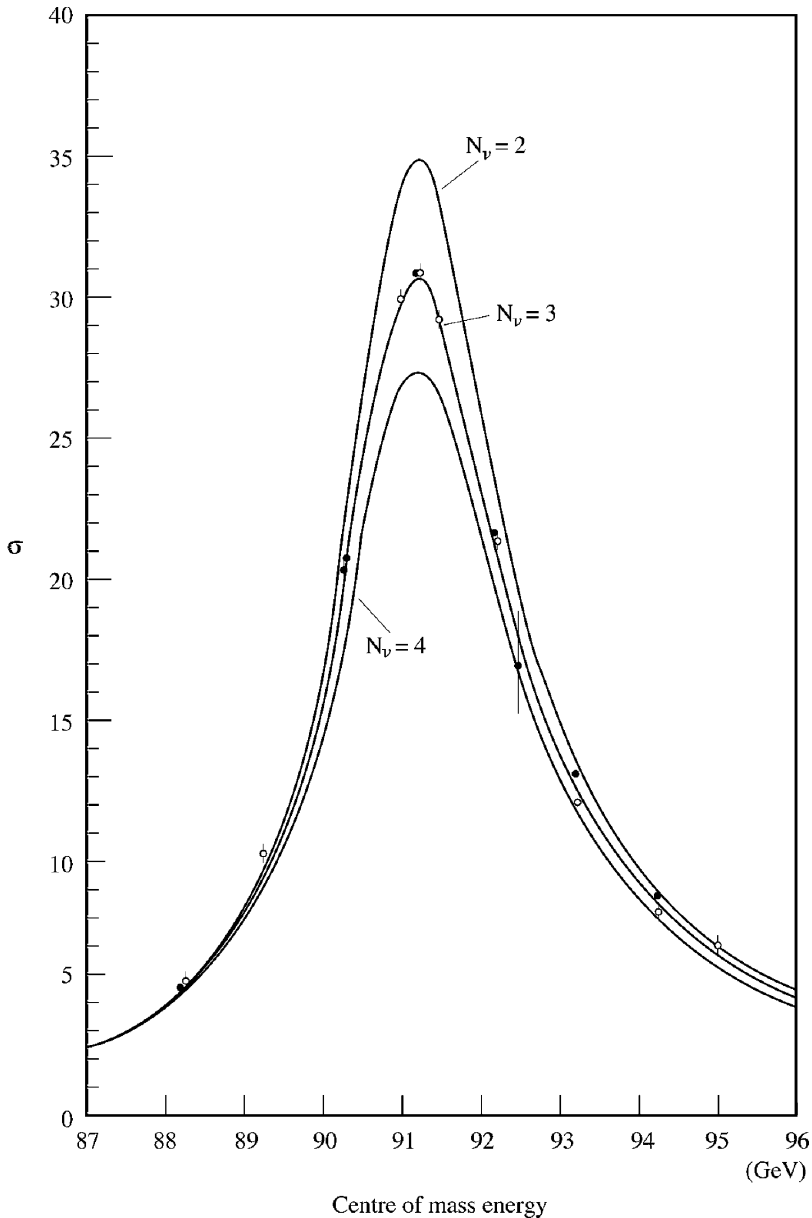


Figure 13.4 The cross-section $\sigma(e^+e^- \rightarrow \text{hadrons})$ as a function of E the initiating e^+e^- centre of mass energy. The experimental data were presented at the 25th International Conference on High Energy Physics in Singapore in 1990 by the OPAL collaboration of CERN. The data are compared with the predictions of the Standard Model but with two, three and four neutrino types. Three light neutrino types are clearly favoured (see Mori (1991)).

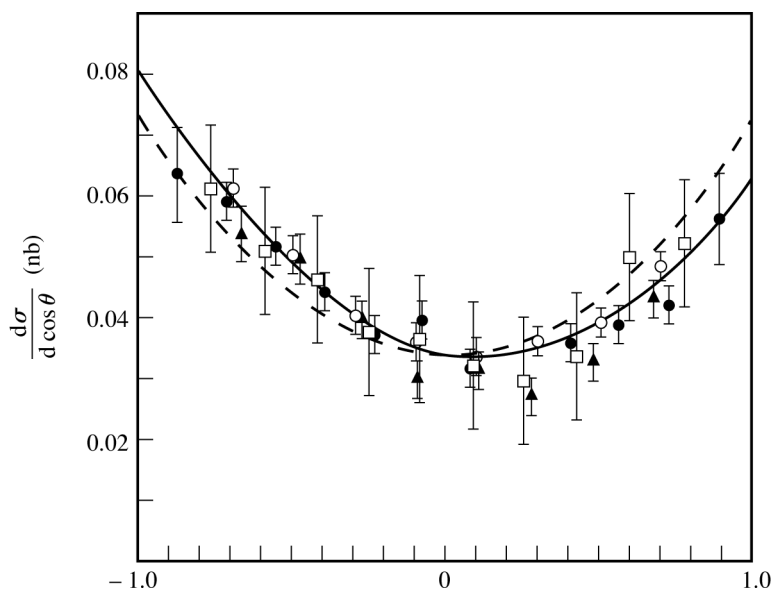


Figure 13.5 The differential cross-section $d\sigma(e^+e^- \rightarrow \mu^+\mu^-)/d\cos\theta$. The data were taken at DESY at an e^+e^- centre of mass energy of 30 GeV. The dashed line is the prediction of quantum electrodynamics alone, the full line fits the data and shows the modification due to the presence of the Z boson which gives this interference effect (R. Marshall, Rutherford Appleton Laboratory Report RAL 89-021).

helicity electrons and positive helicity positrons are associated with left-handed fields, positive helicity electrons and negative helicity positrons are associated with right-handed fields. It follows from the form of the interaction term (12.33) in the Weinberg–Salam Lagrangian that in interacting with an unpolarised positron beam (equal numbers of positive helicity and negative helicity positrons) the cross-section σ_L for Z production by a negative helicity electron is proportional to $(\cos 2\theta_w)^2$ and the cross-section σ_R for Z production by a positive helicity electron is proportional to $(2\sin^2\theta_w)^2$. The constants of proportionality are the same so that the left–right cross-section asymmetry is, to lowest order,

$$A_{LR} = \frac{\sigma_L - \sigma_R}{\sigma_L + \sigma_R} = \frac{(\cos 2\theta_w)^2 - (2\sin^2\theta_w)^2}{(\cos 2\theta_w)^2 + (2\sin^2\theta_w)^2} = \frac{2(1 - 4\sin^2\theta_w)}{1 + (1 - 4\sin^2\theta_w)^2}.$$

From the measurements at SLC (Fero, 1994) it is calculated that $A_{LR} = 0.1628 \pm 0.0099$, which gives an estimate

$$\sin^2\theta_w = 0.2292 \pm 0.0013.$$

This estimate does not depend on the ratio M_w/M_Z , since the W^\pm bosons are not involved.

At CERN and at a previous e^+e^- collider at DESY in Hamburg the electron beams had no longitudinal polarisation. Nevertheless if a Z boson is formed its spin is aligned with the direction of the electron beam with probability proportional to $[2 \sin^2 \theta_w]^2$, and anti-aligned with probability proportional to $[\cos 2\theta_w]^2$, giving it a mean polarisation in the direction of the beam of $-A_{LR}$.

When the Z decays to a lepton–antilepton pair, the direction of the lepton is correlated with the direction of the Z spin. The polarisation of the Z therefore gives a forward–backward asymmetry in the angular distribution of the leptons.

The competing process of lepton production through the electromagnetic interaction does give a symmetrical angular distribution. The observed asymmetry depends on the interference between Z and γ processes, and is energy dependent. Figure 13.5 shows the angular distribution of leptons with respect to the electron beam distribution at a centre of mass energy $E = 30$ GeV (which is below M_Z). This data was taken at DESY and gave an estimate of $\sin^2 \theta_w = 0.212 \pm 0.014$. This is another impressive confirmation of the overall consistency of the Weinberg–Salam theory.

Problems

13.1 W^\pm bosons are produced when a beam of high energy protons is in head-on collision with a beam of antiprotons. The W boson momenta are strongly aligned with the beams. The transverse component of momentum given to the W is small. Neglecting this component, and assuming that in the W rest frame there is an isotropic distribution of decay products, show that in a decay to a charged lepton and a neutrino, the root mean square transverse lepton momentum is approximately $M_w/\sqrt{6} = 33$ GeV.

Events with large transverse momenta are rare, and their observation allows W production to be identified. (Note that the transverse momenta are unchanged by a Lorentz boost of the W in the beam direction.)

13.2 From the interaction term in (12.23) of the Z boson with an electron–positron pair, show that in head-on unpolarised e^+e^- collisions, the probability of the Z boson spin being aligned with the electron beam is proportional to $(2 \sin^2 \theta_w)^2$, and of being antialigned is proportional to $(\cos 2\theta_w)^2$.

13.3 Neglecting lepton mass terms, obtain the partial widths (13.2), (13.3) and (13.4).

13.4 Recalculate (13.3), taking $\cos \theta_w = M_w/M_Z$.